The bromodomain inhibitor JQ1 is a molecular glue targeting centromeres.

Samuel Corless[1,2], Noor Pratap-Singh[3], Nezha S. Benabdallah[4], Jasmin Böhm[1], Alexander M. Simon[1,2], Vojtěch Dolejš[1,2], Simon Anders[2], Ana Banito[4] and Sylvia Erhardt[1,2]*

[1]Karlsruhe Institute of Technology (KIT) - South Campus, Zoological Institute, Molecular Cell Biology, Fritz-Haber-Weg 4, D-76131 Karlsruhe, Germany

[2]University of Heidelberg, Center for Molecular Biology Heidelberg (ZMBH), Im Neuenheimer Feld 282, 69120 Heidelberg, Germany

[3]University of Maryland, Department of Computer Science, College Park, MD 20740, USA

[4]German Cancer Research Center (DKFZ), Soft-Tissue Sarcoma (B380), Im Neuenheimer Feld 581, 69120 Heidelberg, Germany

*Correspondence to: sylvia.erhardt@KIT.edu

Centromeres are the position on each chromosome that orchestrates the accurate partitioning of the genome during cell division. Centromere-dependent cell-cycle checkpoints are maintained by cancer cells to prevent catastrophic chromosome segregation defects in dividing cells[1,2], making centromeric chromatin a valuable target for anti-cancer therapeutics. However, no compounds have been identified that specifically target centromeric chromatin using standard drug discovery approaches. Here we develop a big-data approach to identify the protein composition of repetitive DNA loci, including centromeres, and screen candidate small molecules that act on centromeric chromatin composition. We discover that the BET bromodomain protein BRD4 localises to centromeres and regulates centromeric cohesion. We further show that the bromodomain inhibitor JQ1 affects centromeric BRD4 by stabilising a direct interaction between BRD4 and Centromere Protein B (CENP-B), acting as a molecular-glue that promotes centromere cohesion in a CENP-B-dependent manner. Strikingly, CENP-B transitions from a non-essential protein in JQ1-sensitive cells to the most significant determinant of cell-proliferation in JQ1-resistant cells. Our observations demonstrate a completely overlooked role for BRD4 and JQ1 in directly targeting the centromere, with important consequences for JQ1-derivatives currently entering clinical use[3].

30 Human centromeres have long been considered an enigmatic and challenging region of the
31 genome to study using sequencing-based approaches, due to the highly repetitive nature of their
32 DNA (Fig. 1a)[4]. The function of centromeric loci is to ensure the accurate partitioning of the
33 genome during cell-division by assembling the multi-subunit kinetochore complex, which
34 attaches chromosomes to the spindle microtubules[5,6]. Defects in centromere structure and
35 function are key drivers of aneuploidy, tumour heterogeneity and cancer progression[7,8]. Such
36 diverse roles indicate that centromeric proteins are an attractive target for anti-cancer
37 therapeutics, but there are no known inhibitors that specifically target components of
38 centromeric chromatin. A major barrier to progress in human centromere biology has been the
39 lack of studies mapping chromatin proteins to highly-repetitive DNA regions[9], and for the
40 most-part our understanding of centromeric chromatin remains in the pre-genomic era.

41 In contrast to centromeres, our understanding of chromatin within unique-sequence regions has
42 been revolutionised thanks to the broad application of genome-wide chromatin mapping
43 approaches, which have significantly improved our understanding of the molecular
44 mechanisms of transcription factors[10], regulatory elements[11], 3D genome organisation[12],
45 chromatin-associated disease[13,14] and specific classes of small-molecule inhibitors targeting
46 chromatin components[13]. In these published studies centromeric loci were excluded from the
47 analysis, either through the use of a genome-build in which centromeric repeats are absent or
48 because standard pipelines exclude repetitive DNA[4], but the raw experimental data containing
49 this information is publicly accessible through the Sequence Read Archive (SRA)[15]. We took
50 advantage of this vast resource and developed an approach called Reanalysis of Every Dataset
51 at Positions Of INTerest (REDPOINT) that utilised published chromatin-mapping datasets to
52 identify the protein composition of any locus. The objective of our study was to identify
53 inhibitors that target the protein composition of centromeres. To achieve this, we first analysed
54 the proteins present at centromeric chromatin and then conducted a focused investigation on a
55 subset of REDPOINT data that included small-molecule treatments.

56 Our analysis included 40,733 chromatin immunoprecipitation sequencing (ChIP-seq)
57 experiments that identified the genomic distribution of more than 1200 human chromatin
58 proteins and post-translational modifications (Fig. 1b). The workflow included the following
59 steps: 1) download 100,000 reads per ChIP-seq sample from the SRA, 2) align to a human
60 genome build which includes information for repetitive loci[4], 3) retain repetitive regions and
61 identify the percentage of reads aligned to the centromere compared to the whole genome, 4)
62 repeat for each dataset, 5) annotate and analyse the data. We observe a striking enrichment of

proteins previously identified at the centromere-core which is the site of kinetochore formation and microtubule attachment during chromosome segregation[16] (CENP-A, CENP-B, CENP-C, CENP-T), pericentromeric heterochromatin which supports centromere-core function[17] (HP1α, HP1β, DNMT1, DNMT3A, ATRX) and other proteins with centromeric roles (LRWD1, TRF2, DDX11, TOP2α, HIRA, RAC3, SMAD3, BCL6) (Fig. 1a, c). We also identified 19 high confidence new centromere protein candidates, which met one or both of the following criteria: 1) more than two-fold enriched compared to corresponding control, 2) in the top 500 samples by percent of reads aligned to the centromere. Within the new centromere candidates was BRD4, a key protein in the organization of super-enhancers, transcription elongation and interphase genome organization[18–20].

By analysing a particular subset of the REDPOINT data that contained ChIP-seq samples acquired post-exposure to diverse small-molecule inhibitors, and focusing specifically on 50 protein-inhibitor pairs that were examined in multiple studies, we identified that BRD4-JQ1 is the sole protein-inhibitor pairing that exhibits a highly significant alteration in protein abundance at the centromeric regions across all studies that were analysed (Fig. 1d). JQ1 is a small-molecule BET bromodomain inhibitor that prevents BRD4 from binding its acetyl-chromatin substrate[21], so the canonical mechanism-of-action predicts that JQ1 treatment decreases BRD4 levels at its chromatin binding sites. Unexpectedly, we observe that JQ1 treatment consistently increases BRD4 occupancy at centromeres.

The discovery of the presence and JQ1-induced increase of BRD4 at centromeres is remarkable. Typically, BRD4 is considered as a regulator of genes and enhancers[19], but centromeric regions lack these elements and are mostly transcriptionally inactive[9,22]. Recent studies have revealed that BRD4 also plays a role in the organisation of the interphase genome by promoting cohesin loading at TAD boundaries, indicating a role in contemporary theories of genome organisation through chromatin loop extrusion[12,18,23]. However, a link between BRD4 and centromeric cohesion has not previously been proposed, which led us to investigate the role of BRD4 and the inhibitor JQ1 at centromeres.

91 ***BRD4 regulates centromere cohesion***

92 To visualise the relationship between BRD4 and centromeres in greater detail we mapped
93 BRD4 ChIP-seq reads from diverse cell types onto the telomere-to-telomere (T2T) build of
94 chromosome 8[24]. BRD4 is enriched at many sites, including at centromeric loci defined by the
95 co-localisation with CENP-A and HP1 (Fig. 2a). Immunofluorescence in HeLa cells with
96 antibodies targeting BRD4 and CENP-A revealed a clear co-localisation of these proteins as
97 puncta within the DAPI dense heterochromatin at the periphery of nucleoli (Fig. 2b), indicating
98 that BRD4 is a centromere-core protein not enriched in adjacent pericentromeric
99 heterochromatin.

100 Centromeres have unique chromatin properties that differ markedly from gene-rich regions,
101 including low levels of histone acetylation and transcription[22,25,26], indicating a non-canonical
102 role for BRD4 at centromeric chromatin. We first confirmed that centromeric BRD4
103 enrichment does not correspond to an enrichment in H3K27ac or RNA polymerase II (Fig. 2a,
104 c). Next we completely depleted BRD4 from cells using MZ1, a proteolysis-targeted chimera
105 (PROTAC) small-molecule that selectively degrades BRD4 when compared to BET
106 bromodomains paralogs BRD2 and BRD3[27]. Unlike the bromodomain inhibitors PFI1 and the
107 racemic mixture of (±)-JQ1 (referred to as JQ1), MZ1 treatment leads to the complete loss of
108 BRD4 protein from the cell (Fig. 2d), including at the centromere core (Fig. 2e, f). We then
109 quantified the effect of BRD4 degradation on centromere cohesion defects in metaphase
110 chromosomes prepared from HEK293T and Hela cells, using a scale ranging from partial
111 centromere defect to complete cohesion failure (Fig. 2g). This revealed that MZ1 treatment led
112 to a highly significant increase in centromere cohesion defects (Fig. 2h). These results identify
113 a previously uncharacterised role for BRD4 in the organisation of centromere cohesion and
114 demonstrate that PROTAC inhibitors targeting BRD4 strongly disrupt metaphase chromosome
115 architecture in different cell types (Fig. 2i).

116

117 ***JQ1 promotes BRD4 at centromeres***

118 To understand why JQ1 promotes BRD4 localisation to centromeres (Fig. 1d) we investigated
119 in more detail data from 15 different studies with 26 different cell-lines (Fig. 3a, b). In all
120 studies and in 25 of 26 cell-lines BRD4 increased at the centromere following JQ1, with the
121 JQ1-resistant cell-line SUM149R being the only exception. This recruitment was specific to
122 BRD4 and to centromeres, since other bromodomain proteins did not show the same level of

123 centromere accumulation (Extended Data Fig. 1a) and BRD4 was not enriched at abundant
124 LINE2 repetitive DNA elements following JQ1 treatment (Extended Data Fig. 1a, b). To
125 confirm this specificity, we plotted the fold-change in BRD4 localisation following JQ1
126 treatment on a T2T genome and observed that the centromere is the principle locus gaining
127 BRD4 association in different cell lines (Fig. 3c). Importantly, JQ1 treatment did not
128 significantly increase H3K27ac, RNA polymerase II or centromeric transcription ruling out a
129 JQ1-dependent switch to the canonical functions of acetylation-dependent transcriptional
130 control at centromeres (Fig. 3c, d, Extended Data Fig. 1a, c).

131 To consider non-canonical effects of JQ1 treatment we again quantified centromere cohesion
132 defects in metaphase chromosomes prepared from HEK293T and Hela cells. In contrast to
133 PROTAC-based degradation, JQ1 treatment identified fewer centromere cohesion defects (Fig.
134 3e). HEK293T cells show a significant transition towards milder defects ('mixed' phenotype).
135 More strikingly, the proportion of HeLa cells with chromosome defects following JQ1
136 treatment was comparable to DMSO (Fig. 2h, 3e), suggesting the possibility that BRD4
137 recruitment stabilises centromeric chromatid cohesion (Fig. 3f).

138

139 ***JQ1 stabilises an interaction between BRD4 and CENP-B***

140 To further characterise the effect of JQ1 treatment on BRD4 at centromeres we performed
141 immunofluorescence and observed no large-scale reorientation of BRD4 towards centromeric
142 loci (Extended Data Fig. 2a, b), reflecting the subtle yet significant change in BRD4 observed
143 by REDPOINT (Fig. 3b) and highlighting the higher sensitivity of our approach to determine
144 novel chromatin interactions than can be achieved by microscopy-based screens.

145 To investigate at the molecular scale how BRD4 is further recruited to and maintained at the
146 centromere upon JQ1 treatment we analysed published co-IP mass spectrometry (coIP-MS)
147 data identifying the proteins which specifically interact with BRD4 following JQ1
148 treatment[28,29]. JQ1 treatment consistently induced a strong, and previously overlooked,
149 association between BRD4 and key centromere proteins (Fig. 4a, Extended Data Fig. 2c, d).
150 Across all four cell-types assayed, and in as little as 10 minutes following JQ1 addition, a new
151 top interaction between BRD4 and the constitutive centromere protein CENP-B formed (Fig.
152 4a, Extended Data Fig. 2c, d). Co-IP MS for other BET proteins show a low-affinity (BRD3)
153 or no (BRD2) interaction with CENP-B following JQ1 (Extended Data Fig 2e). Members of
154 the MIS18 complex (MIS18A, MIS18B and MIS18BP1), which binds the centromere for a few

155 minutes each anaphase to licence the deposition of CENP-A[30], were also highly enriched in
156 coIP-MS experiments but considered unlikely to be the major factor recruiting BRD4 to the
157 centromere due to the transient nature of this interaction.

158 CENP-B is the only well characterised centromere-specific DNA binding protein, and binds
159 throughout the cell-cycle to a 17 base-pair CENP-B box DNA sequence found on every
160 centromere except the Y-chromosome[31]. We observe a strong positive correlation between the
161 level of CENP-B binding at a centromere and the recruitment of BRD4 following JQ1
162 treatment (Extended Data Fig. 3a). In fact, JQ1 treatment recruits BRD4 to all centromeres
163 except the Y chromosome (4 out of 5 male cell-lines investigated) (Fig. 4b, Extended Data Fig.
164 3b, c). No correlation was found between CENP-B and RNA polymerase II following JQ1
165 treatment, or BRD4 following degradation with the PROTAC inhibitor dBET6 (Extended Data
166 Fig. 3d). Together, these observations strongly support CENP-B as the key protein mediating
167 the JQ1-dependent recruitment of BRD4 to centromeres.

168 We independently confirmed a strong and specific JQ1-dependent interaction between BRD4
169 and CENP-B in HeLa and HEK293T cells by co-IP western blot (Fig. 4c, Extended Data Fig.
170 4a, b), which was not observed in co-IP following treatment with the negative enantiomer (–)-
171 JQ1[32] or the BET bromodomain inhibitor PFI1[33] which has a different chemical structure
172 (Extended Data Fig. 4c).

173 To identify whether the JQ1-dependent interplay between BRD4 and CENP-B is direct, we
174 reconstituted the interaction *in vitro* using full-length CENP-B and the bromodomains of BRD4
175 ($BRD4^{bromo}$) (Fig. 4d). We observed that CENP-B protein was strongly associated with the
176 CENP-B box DNA sequence when compared to a shuffled version of the same sequence (Fig.
177 4 e, f). The addition of (+)-JQ1 or (–)-JQ1 enantiomer to CENP-B alone did not change the
178 level of interaction with the CENP-B box DNA sequence, indicating that these small-molecules
179 have no effect on CENP-B-DNA interactions alone. $BRD4^{bromo}$ was enriched in the presence
180 of CENP-B bound CENP-B box DNA compared to shuffled DNA, even with the (–)-JQ1
181 enantiomer, indicating that a low-affinity complex between BRD4 and CENP-B occurs
182 independently of the BRD4-JQ1 association *in vitro*. However, with the addition of the (+)-
183 JQ1 enantiomer, $BRD4^{bromo}$ and CENP-B became significantly more enriched, indicating that
184 (+)-JQ1 stabilises the BRD4-JQ1-CENP-B-DNA complex *in vitro*. The stabilisation of a low-
185 affinity interaction is one of the defining properties of a rare class of inhibitors called
186 molecular-glues, which enable gain-of-function interactions that can target previously

187 undruggable pathways[34,35], and our evidence suggests that (+)-JQ1 is the first centromere-
188 targeting small-molecule via this mechanism-of-action.

189

190 ***BRD4-JQ1-CENP-B stabilises centromere cohesion***

191 If the BRD4-JQ1-CENP-B complex stabilises the centromere cohesion role of BRD4,
192 removing CENP-B and treating cells with JQ1 should give centromere cohesion defects
193 comparable to MZ1 treatment (Fig. 4g). To test this hypothesis, we generated HEK293T and
194 HeLa cells lacking CENP-B through a CRISPR knock-out (CENP-B KO) approach (Fig. 4h,
195 Extended Data Fig. 5a). In HEK293T CENP-B KO cells we observed a marginal enhancement
196 of the already apparent cohesion defect following JQ1 treatment (Extended Data Fig. 5b).
197 However, in HeLa CENP-B KO cells we observed a massive increase in centromere cohesion
198 defects compared to control cells, comparable to the degradation of BRD4 and consistent with
199 our proposed model (Fig. 4i). These observations indicate that JQ1 has a cell-type variable role
200 in targeting centromere structure and function, through a novel complex between CENP-B and
201 BRD4.

202 Interestingly, among the 26 different cell lines analysed in this study, only the JQ1-resistant
203 cell-line SUM149R[28,36] did not show an increase in centromere localised BRD4 following JQ1
204 treatment (Fig. 3b). SUM149R cells were selected in increasing concentrations of JQ1 and now
205 grow more rapidly in the presence of JQ1 than in DMSO[36]. To determine whether the
206 mechanism of resistance is SUM149R cells is linked to CENP-B, we analysed a published
207 CRISPR-KO screen in parental and resistant cells treated with DMSO or JQ1[28]. CENP-B is a
208 non-essential protein in SUM149 (wild-type) cells treated with DMSO or JQ1 because knock-
209 out does not significantly alter cellular proliferation, consistent with published observations
210 including viable CENP-B KO mice[37]. In contrast, SUM149R (JQ1 resistant) cells are highly
211 sensitive to the loss of CENP-B protein (Fig. 4j). In rapidly growing SUM149R-JQ1 cells,
212 CENP-B KO reduces cell proliferation, whereas in slowly growing SUM149R-DMSO cells,
213 CENP-B KO gives the most significant increase in cell proliferation out of 18,461 proteins
214 tested. We identified no other protein with a similar response amongst BET bromodomain
215 proteins, transcription elongation components, cohesin complex components or components of
216 centromeric chromatin (Extended Data Fig. 5c). These observations suggest that CENP-B
217 specifically regulates cell proliferation in a cellular model of JQ1 resistance and indicates that
218 the BRD4-JQ1-CENP-B complex is critical in establishing JQ1 resistance.

219 **Discussion**

220 In summary, our study identified a previously overlooked role for BRD4 and the bromodomain
221 inhibitor JQ1 in centromere cohesion. We demonstrated JQ1 as the first small-molecule
222 directly targeting centromeric chromatin, through a molecular-glue mechanism-of-action that
223 stabilises a link between BRD4 and CENP-B. The identification of molecular glues is rare, but
224 each new example opens up the possibility of targeting previously undruggable pathways[34,35].
225 Future optimisation of JQ1 structure could form the basis of a new class of centromere drugs
226 targeting chromosome segregation, a process which is important only in dividing cells. We
227 showed that the BRD4-JQ1-CENP-B interaction stabilises centromere cohesion in mitosis,
228 supporting a direct role for BRD4 in centromere cohesion and complementing recent
229 observations that identified a role for BRD4 in regulating TADs by acting upstream of cohesin
230 loading[18,38]. Finally, we show that CENP-B transitions from non-essential in JQ1-sensitive
231 cells to the most significant determinant of cell proliferation in JQ1-resistant cells. A
232 significant challenge in employing BET bromodomain inhibitors for cancer treatment is the
233 swift emergence of resistance[3,39], and our observations show that this resistance can occur via
234 mechanisms independent of gene-regulation. Future bromodomain inhibitors developed for
235 clinical use must consider this centromere role, in order to better target cancer-cell pathways
236 and avoid mechanisms of resistance linked to CENP-B.

237

238 **References**

239 1. Cohen-Sharir, Y. *et al.* Aneuploidy renders cancer cells vulnerable to mitotic checkpoint
240 inhibition. *Nature* **590**, 486–491 (2021).

241 2. Matthews, H. K., Bertoli, C. & de Bruin, R. A. M. Cell cycle control in cancer. *Nat Rev*
242 *Mol Cell Biol* **23**, 74–88 (2022).

243 3. Trojer, P. Targeting BET Bromodomains in Cancer. *Annu. Rev. Cancer Biol.* **6**, 313–336
244 (2022).

245 4. Miga, K. H. The Promises and Challenges of Genomic Studies of Human Centromeres.
246 *Prog. Mol. Subcell. Biol.* **56**, 285–304 (2017).

247 5. Allshire, R. C. & Karpen, G. H. Epigenetic regulation of centromeric chromatin: old dogs,
248 new tricks? *Nat. Rev. Genet.* **9**, 923–937 (2008).
249 6. Black, B. *Centromeres and kinetochores: discovering the molecular mechanisms*
250 *underlying chromosome inheritance*. (Springer, 2017).
251 7. Barra, V. & Fachinetti, D. The dark side of centromeres: types, causes and consequences
252 of structural abnormalities implicating centromeric DNA. *Nat Commun* **9**, 4340 (2018).
253 8. Jeffery, D. *et al.* CENP-A overexpression promotes distinct fates in human cells, depending
254 on p53 status. *Commun Biol* **4**, 417 (2021).
255 9. Altemose, N. *et al.* Complete genomic and epigenetic maps of human centromeres. *Science*
256 **376**, eabl4178 (2022).
257 10. Lambert, S. A. *et al.* The Human Transcription Factors. *Cell* **175**, 598–599 (2018).
258 11. Panigrahi, A. & O'Malley, B. W. Mechanisms of enhancer action: the known and the
259 unknown. *Genome Biol* **22**, 108 (2021).
260 12. Rao, S. S. P. *et al.* Cohesin Loss Eliminates All Loop Domains. *Cell* **171**, 305-320.e24
261 (2017).
262 13. Valencia, A. M. & Kadoch, C. Chromatin regulatory mechanisms and therapeutic
263 opportunities in cancer. *Nat Cell Biol* **21**, 152–161 (2019).
264 14. Mitchener, M. M. & Muir, T. W. Oncohistones: Exposing the nuances and vulnerabilities
265 of epigenetic regulation. *Mol Cell* **82**, 2925–2938 (2022).
266 15. Katz, K. *et al.* The Sequence Read Archive: a decade more of explosive growth. *Nucleic*
267 *Acids Res* **50**, D387–D390 (2022).
268 16. Kixmoeller, K., Allu, P. K. & Black, B. E. The centromere comes into focus: from CENP-
269 A nucleosomes to kinetochore connections with the spindle. *Open Biol* **10**, 200051 (2020).
270 17. Janssen, A., Colmenares, S. U. & Karpen, G. H. Heterochromatin: Guardian of the
271 Genome. *Annu. Rev. Cell Dev. Biol.* **34**, 265–288 (2018).

272 18. Linares-Saldana, R. *et al.* BRD4 orchestrates genome folding to promote neural crest
273 differentiation. *Nat Genet* **53**, 1480–1492 (2021).
274 19. Altendorfer, E., Mochalova, Y. & Mayer, A. BRD4: a general regulator of transcription
275 elongation. *Transcription* **13**, 70–81 (2022).
276 20. Eagen, K. P. BET proteins loop and compartmentalize the 3D genome. *Nat Genet* **54**, 370–
277 371 (2022).
278 21. Filippakopoulos, P. & Knapp, S. Targeting bromodomains: epigenetic readers of lysine
279 acetylation. *Nat Rev Drug Discov* **13**, 337–356 (2014).
280 22. Hoyt, S. J. *et al.* From telomere to telomere: The transcriptional and epigenetic state of
281 human repeat elements. *Science* **376**, eabk3112 (2022).
282 23. Olley, G. *et al.* Publisher Correction: BRD4 interacts with NIPBL and BRD4 is mutated in
283 a Cornelia de Lange-like syndrome. *Nat Genet* **51**, 1192 (2019).
284 24. Logsdon, G. A. *et al.* The structure, function and evolution of a complete human
285 chromosome 8. *Nature* **593**, 101–107 (2021).
286 25. Corless, S., Höcker, S. & Erhardt, S. Centromeric RNA and Its Function at and Beyond
287 Centromeric Chromatin. *J Mol Biol* **432**, 4257–4269 (2020).
288 26. Sullivan, B. A. & Karpen, G. H. Centromeric chromatin exhibits a histone modification
289 pattern that is distinct from both euchromatin and heterochromatin. *Nat. Struct. Mol. Biol.*
290 **11**, 1076–1083 (2004).
291 27. Zengerle, M., Chan, K.-H. & Ciulli, A. Selective Small Molecule Induced Degradation of
292 the BET Bromodomain Protein BRD4. *ACS Chem Biol* **10**, 1770–1777 (2015).
293 28. Shu, S. *et al.* Synthetic Lethal and Resistance Interactions with BET Bromodomain
294 Inhibitors in Triple-Negative Breast Cancer. *Mol Cell* **78**, 1096-1113.e8 (2020).
295 29. Lambert, J.-P. *et al.* Interactome Rewiring Following Pharmacological Targeting of BET
296 Bromodomains. *Mol Cell* **73**, 621-638.e17 (2019).

297 30. Fujita, Y. *et al.* Priming of centromere for CENP-A recruitment by human hMis18alpha,
298 hMis18beta, and M18BP1. *Dev Cell* **12**, 17–30 (2007).
299 31. Gamba, R. & Fachinetti, D. From evolution to function: Two sides of the same CENP-B
300 coin? *Exp Cell Res* **390**, 111959 (2020).
301 32. Filippakopoulos, P. *et al.* Selective inhibition of BET bromodomains. *Nature* **468**, 1067–
302 1073 (2010).
303 33. Picaud, S. *et al.* PFI-1, a highly selective protein interaction inhibitor, targeting BET
304 Bromodomains. *Cancer Res* **73**, 3336–3346 (2013).
305 34. Wu, H. *et al.* Molecular glues modulate protein functions by inducing protein aggregation:
306 A promising therapeutic strategy of small molecules for disease treatment. *Acta Pharm Sin*
307 *B* **12**, 3548–3566 (2022).
308 35. Schreiber, S. L. The Rise of Molecular Glues. *Cell* **184**, 3–9 (2021).
309 36. Shu, S. *et al.* Response and resistance to BET bromodomain inhibitors in triple-negative
310 breast cancer. *Nature* **529**, 413–417 (2016).
311 37. Hudson, D. F. *et al.* Centromere protein B null mice are mitotically and meiotically normal
312 but have lower body and testis weights. *J Cell Biol* **141**, 309–319 (1998).
313 38. Xie, L. *et al.* BRD2 compartmentalizes the accessible genome. *Nat Genet* **54**, 481–491
314 (2022).
315 39. Shorstova, T., Foulkes, W. D. & Witcher, M. Achieving clinical success with BET
316 inhibitors as anti-cancer agents. *Br J Cancer* **124**, 1478–1490 (2021).
317
318
319

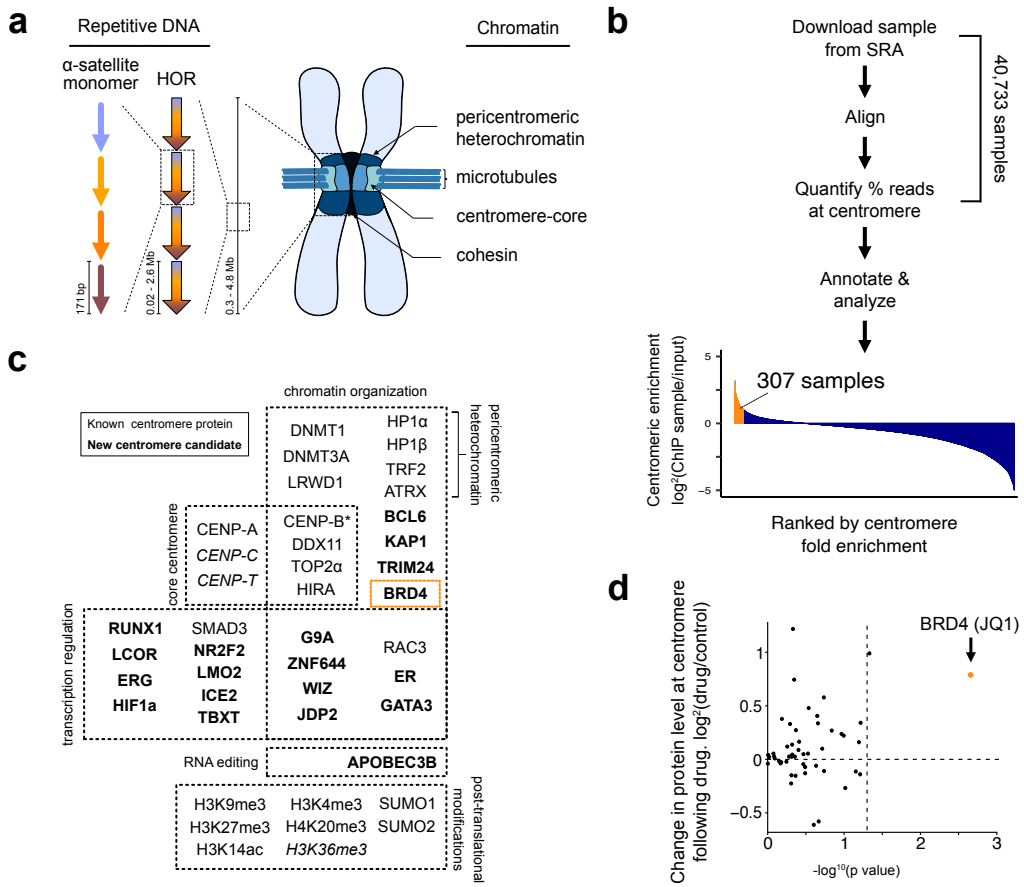

Fig. 1 | BRD4 is a centromere protein which is further enriched by the bromodomain inhibitor JQ1. a, Overview of human centromeric DNA organisation and the subdomains of centromeric chromatin displayed on metaphase chromosomes. Length of DNA repeat motifs given in base-pairs (bp) and Megabases (Mb). **b**, Summary of the REDPOINT workflow for centromeric loci. **c**, REDPOINT identifies 35 high confidence centromere proteins including known and novel candidates. Protein categories were determined from published data and Uniprot information. *CENP-B was identified using the same pipeline to analyse a published CUT&RUN dataset PRJNA546288. **d**, Focused analysis of 50 different protein-inhibitor pairs investigated in multiple studies and identified through the REDPOINT approach. The x-axis is the statistical significance from a paired-sample t-test comparing centromeric protein abundance in inhibitor treatment to control across multiple studies, with the vertical dotted line signifying a p-value of 0.05. The y-axis is the fold-change in protein abundance at the centromere following inhibitor treatment, with a positive fold change indicating more protein at the centromere and a negative fold change indicating less protein at the centromere.

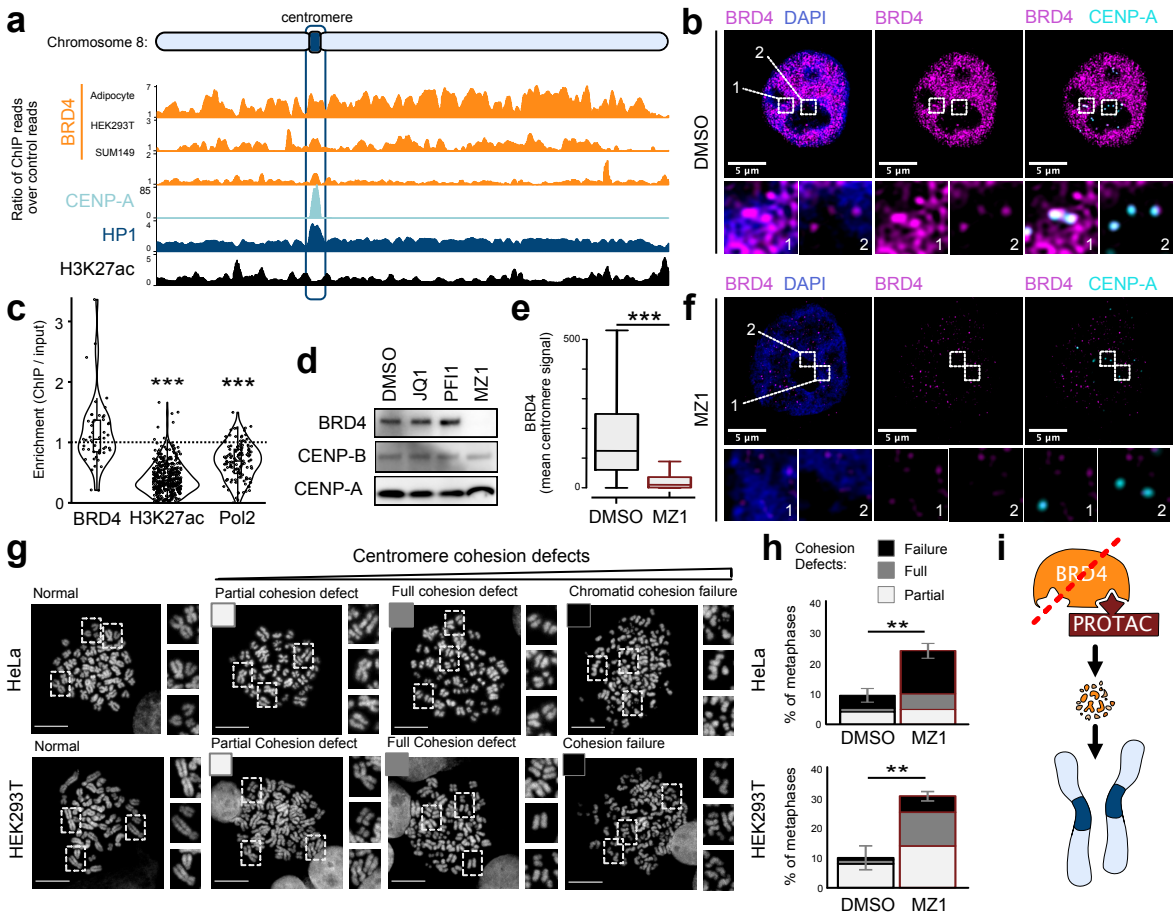

Fig. 2 | BRD4 degradation disrupts mitotic centromere cohesion. a, Telomere-to-telomere distribution of BRD4, CENP-A, HP1 and H3K27ac on chromosome 8. Data displays the ratio of ChIP reads compared to a matched input from the same study. Datasets: CENP-A (HeLa) PRJNA183936, BRD4 and HP1 (HEK293) PRJNA171165, H3K27ac and BRD4 (SUM149) PRJNA268319, BRD4 (adipocyte) PRJNA270506. **b**, Immunofluorescence imaging of BRD4 (magenta) and CENP-A (cyan) in HeLa cells treated for 24 hours with DMSO. **c**, Centromere enrichment of all BRD4, H3K27ac and RNA polymerase II (Pol2) ChIP-seq samples in the REDPOINT dataset compared to the corresponding control from the same study. Statistical analysis t-test between BRD4 and H3K27ac/Pol2 (*** $p<0.001$). **d**, Western blot analysis of BRD4, CENP-A and CENP-B following 24 hours treatment with two bromodomain inhibitors ((±)-JQ1 and PFI1) and the BRD4-specific PROTAC MZ1. **e**, Quantification of BRD4 signal

intensity at the core-centromere in HeLa cells following 24 hours DMSO or MZ1 treatment. Values are the intensity of BRD4 signal overlapping with foci of CENP-A. DMSO (n=3707 centromeres), MZ1 (n=3505 centromeres). Whiskers = boxplot standard in R (1.5x IQR). Statistical analysis t-test (*** $p<0.001$). **f**, Immunofluorescence imaging of BRD4 (magenta) and CENP-A (cyan) in HeLa cells treat following 24 hours MZ1 treatment. Brightness/contrast settings the same as Fig. 1b. **g**, Representative mitotic chromosomes from HeLa and HEK293T cells with normal morphology and increasing severity of centromere cohesion defect. Identifier for subsequent quantifications in inset boxes. **h**, Quantification of mitotic chromosome defects following 24 hours MZ1 treatment in HEK293T and HeLa cells. Error bars = standard error of the mean. Statistical analysis based on triplicate experiments, t-test (** $p < 0.01$). **i**, Model outlining the effect of BRD4 degradation on mitotic chromosome structure.

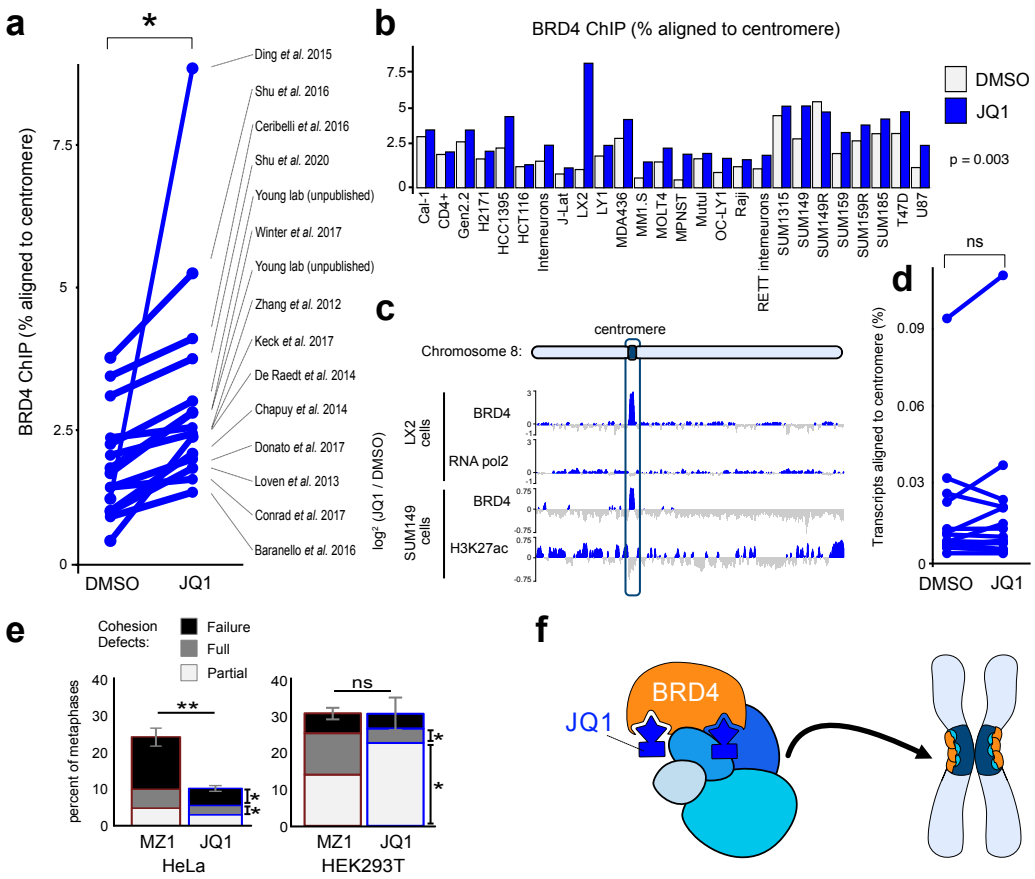

Fig. 3 | JQ1 promotes a non-canonical cohesion function of BRD4 at centromeres. a, Analysis of 15 different ChIP-seq datasets from studies comparing BRD4 distribution in control and JQ1 treated cells. Paired t-test p value < 0.05. **b**, BRD4 is more enriched following JQ1 treatment in 25 out of 26 analysed cell lines. Statistical analysis paired-sample t-test (p=0.003). **c**, BRD4, RNA polymerase II and H3K27ac enrichment following JQ1 compared to DMSO treatment aligned to the T2T genome of chromosome 8. LX2 data from PRJNA253142, SUM149 data from PRJNA542646. **d**, Meta-analysis of RNA-seq datasets comparing DMSO and JQ1 treatment from 12 studies. **e**, Quantification of mitotic chromosome defects following 24 hours MZ1 or (±)-JQ1 treatment in control HEK293T and HeLa cells. Indicator as outlined in Fig. 2g. Error bars = standard error of the mean. Statistical analysis based on triplicate experiments, t-test (ns 'not significant', * p<0.05, ** p<0.01). **f**, Model outlining the rescue of centromere cohesion defects in JQ1-treated cells that recruit BRD4 to the centromere.

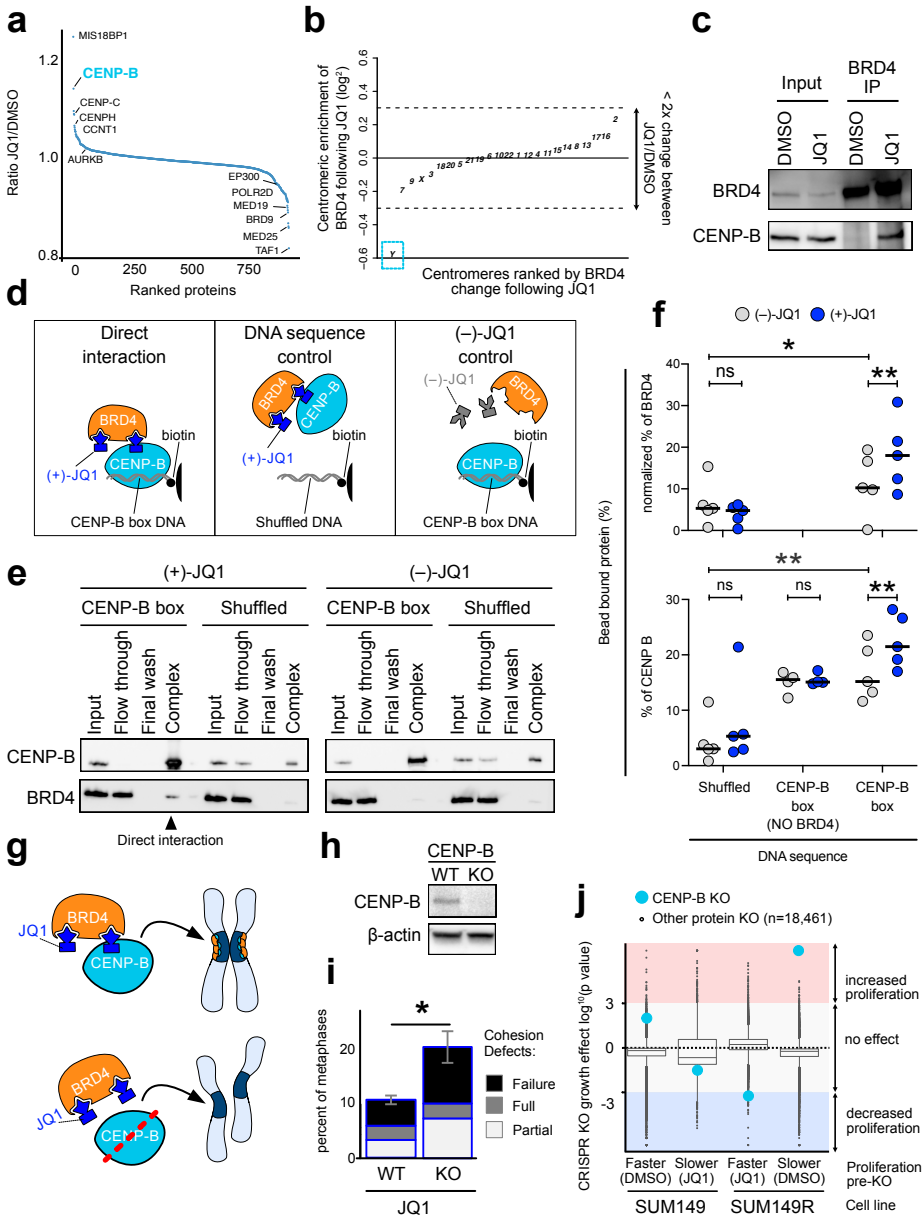

Fig. 4 | JQ1 is a molecular glue that retains BRD4 at centromeres through CENP-B. a, Co-IP MS identifying the change in proteins interacting with BRD4 following JQ1 treatment, with key proteins for centromere identity and BRD4-mediated transcription regulation highlighted. Data from Shu et al. (2020)[28]. **b**, ChIP-seq analysis of centromeres ranked by BRD4 enrichment following JQ1 treatment in male cells. Enrichment was calculated by identifying the percentage of centromeric BRD4 at each chromosome in a sample, and then calculating the ratio of JQ1 treated sample compared to DMSO treated sample. The dotted lines indicate a 2x change in the abundance of a BRD4 at a centromere, the blue square highlights the Y chromosome. Data from: PRJNA253142. **c**, Co-IP for BRD4 following DMSO or (±)-JQ1 treatment for 1 hour in HeLa cells, followed by western blot for BRD4 and CENP-B. **d**,

402 Model outlining an *in vitro* reconstitution pull-down experiment to determine whether a direct
403 interaction occurs between $BRD4^{bromo}$, (+)-JQ1 and CENP-B, with control experiments
404 containing (–)-JQ1 or shuffled DNA sequence. **e**, Example *in vitro* reconstitution pull-down
405 experiment result comprised of western blots of BRD4 and CENP-B. BRD4 is at 10x molar
406 excess compared to CENP-B. 'Input' is 10% of the total sample and 'flow through'/'wash' is
407 10% of the total. 'complex' is 100% of the bead bound protein. **f**, Quantification of independent
408 *in vitro* reconstitution pull-down experiments. To account for the ten-fold molar excess of
409 BRD4 the 'Bead bound protein (% input)' for BRD4 was multiplied by ten to give the
410 'Normalized bead bound protein (%)'. Statistical tests are paired-sample t-test (* $p<0.05$, **
411 $p<0.01$). **g**, Model outlining the predicted outcome of CENP-B loss on JQ1-linked centromere
412 cohesion. **h**, Western blot of control (WT) and CENP-B KO HeLa cells probed with anti-
413 CENP-B antibodies and β-actin as loading control. **i**, Quantification of cohesion defects in 24
414 hours (±)-JQ1 treated HeLa control and CENP-B KO cells. Error bars = standard error of the
415 mean. Statistical analysis based on triplicate experiments t-test (* $p<0.05$). **j**, CRISPR KO
416 screen comparing the effect of CENP-B KO relative to 18,460 other proteins on cellular
417 proliferation in JQ1-sensitive and -resistance SUM149 breast cancer cells. Data from Shu et al.
418 (2020).

419

420

421

422

423

424

425

426

427

428

429

430

431 **Methods**

432 ***Candidate identification with REDPOINT***

433 *Dataset curation for analysis by REDPOINT*

434 A list of human ChIP-seq accession numbers, which allow dataset recovery from the Sequence
435 Read Archive (SRA)[1], were obtained using the 'advanced search' feature of the European
436 Nucleotide Archive (ENA) (https://www.ebi.ac.uk/ena/browser/advanced-search) with the
437 search parameters: Data type = 'Raw reads', Taxon name = 'Homo sapiens', Library Strategy
438 = 'ChIP-seq', and the field parameters: 'experiment accession' and 'sample accession'. The
439 'sample accession' enabled each dataset to be downloaded from the SRA, and the 'experiment
440 accession' allowed the samples from the same study to be grouped in downstream analyses.
441 The state of sample annotation within the SRA, ENA or the Gene Expression Omnibus (GEO)
442 did not allow for automated annotation of key features for our study, including whether the
443 sample was from a ChIP-seq experiment or corresponding input/control, the protein enriched
444 by the ChIP-seq experiment, the tissue/cell-line investigated, whether the sample was treated
445 with a drug or other experimental perturbation, and the associated PubMed ID. To enable
446 detailed downstream analysis of protein enrichment relative to corresponding input/control, the
447 influence of cell/tissue type, and the effect of perturbations including drug treatment, the first
448 21,462 samples from 1,234 studies were annotated by hand using the relevant parameters
449 included with the samples GEO submission.

450

451 *Genomic positions investigated by REDPOINT*

452 We used the hg38 genome build, which contains the entire human genome including
453 representative maps of repetitive regions, from which we extracted centromeric and LINE2
454 alignment information[2].

455

456 *Detailed description of centromeric loci*

457 Centromeric repeats, are annotated in the hg38 genome and in recently published T2T
458 genomes[2–4]. In hg38 centromeric DNA is divided into different classes of satellite repeat,
459 including the dominant α-satellite repeat found at the centromere on every chromosome and
460 low abundance satellite classes which are each found at a small number of centromeres (GSAT,

461 GSATII, GSATX, HSAT4, SST1). The CENP-A-containing core centromere has only been
462 shown to form on the dominant α-satellite DNA[3]. α-satellite is highly divergent and has
463 different Higher Order Repeats (HORs) on different chromosomes[3]. In hg38 the centromeric
464 α-satellite repeats are sub-divided into different chromosomes based on the abundance of
465 different HORs, which allows the chromosome-specific abundance of centromeric proteins to
466 be determined from ChIP-seq data and demonstrates the detailed nature of the centromeric
467 annotation in this genome build. Recently, telomere-to-telomere (T2T) builds of the human
468 genome, with the centromeric sequence in the correct linear order across the entire domain for
469 an individual pseudo-haploid genome, have been published[3,4]. Between cell-
470 lines/chromosomes/individuals there is a strong divergence in the position and abundance of
471 different α-satellite HORs, as well as different epi-allele positioning of key centromere proteins
472 including CENP-A within the α-satellite DNA, and mapping short-read ChIP-seq data from a
473 diversity of sources to the complete T2T genome provides little extra positional information
474 compared to the hg38 genome. We therefore identified candidate proteins using the hg38
475 genome, some of which we validate by aligning to a T2T genome.

476

477 *REDPOINT analysis*

478 The REDPOINT pipeline utilises standard bioinformatic tools for data acquisition, genome
479 alignment and genomic position investigation. Briefly, 1.) For each sample, as determined by
480 the SRA 'sample accession', we downloaded a sub-set of 100,000 reads using 'fastq-dump'
481 from NCBI SRA Tools (parallel-fastq-dump -sra-id SAMPLE_ID --threads 4 --outdir out/ --
482 split -3 --gzip). The -3 split argument automatically differentiates between single-end and
483 paired-end sequencing. For consistency across the analysis, and because our analysis focuses
484 on highly repetitive DNA, we only utilised the first read of paired-end sequencing in
485 downstream analysis. We selected reads starting at read 10,000 to avoid observed problems at
486 the start of a file and obtain a random assortment of reads
487 (https://edwards.flinders.edu.au/fastq-dump/). In all cases where we compared a sample sub-
488 set aligned to the complete sequencing run we observed an exact correspondence in the
489 percentage of reads at the centromere, indicating that 100,000 reads are sufficient to identify
490 protein enrichment for a locus comprising 2.15% of the genome without generating sampling
491 bias. 2) We used Bowtie2[5] (ver.2.3.0) to align reads to the hg38 build of the human genome
492 using default settings. 3) We identified the percentage of reads at each genomic position (e.g.

493 centromeric loci, ACTB gene promoter, etc.) using HTseq[6]. This information was recorded and
494 then the loop re-set to begin the next ChIP-seq dataset.

495

496 *Quality control of ranked protein enrichment*

497 The first method utilised for identifying the proteins associated with different loci of interest
498 was to rank samples based on the percentage of ChIP-seq reads associated with each locus.
499 This allowed the use of the full 40,734 samples analysed in the REDPOINT approach and
500 identified well characterised proteins associated with centromeric chromatin. We also noted
501 many examples of artefact proteins enriched via this approach. For example, there were
502 samples which were very highly enriched at centromeric loci, comparable to key CENP
503 proteins, but upon further inspection showed no enrichment compared to control samples
504 within the same study – indicative of a problem with the entire study rather than a new
505 centromeric protein. This suggested to us that the 'ranked data' approach was sufficient to
506 identify candidate proteins, but could be improved upon by comparing samples to
507 corresponding input/control.

508

509 *Quality control of fold-enriched proteins*

510 The second method for identifying the proteins associated with different loci of interest had a
511 number of quality control steps which take advantage of the 21,462 annotated ChIP-seq
512 samples. Input and control samples provided an invaluable quality control metric, firstly to
513 exclude problematic datasets and secondly to benchmark the proportion of centromeric DNA
514 identified in the samples within a study, which varied by around four-fold from around 1% to
515 around 4% for the majority of samples. Analysis of genomic DNA samples in the same cell
516 line across multiple studies suggested that these differences reflects inter-study variability,
517 rather than biological variability, which may be linked to differential PCR efficiency of highly
518 repetitive loci or variability in the loss of highly compact centromeric chromatin dependent on
519 the methodology used for genomic DNA or control preparation[7]. Many studies did not include
520 a genomic input sample, IgG pull-down or other corresponding control and we excluded these,
521 retaining 11,881 samples from 887 studies. Focussing on the genomic DNA or control samples
522 in these studies, we noted that a sub-set of these samples contained virtually no DNA which
523 aligned to centromeric loci. This is not biologically possible and suggests a technical problem

524 with these samples, which may reflect experimental issues or mistakes in data handling. We
525 removed all studies with fewer than 1% of the reads aligned to centromeric DNA which left us
526 with 9,764 samples from 780 studies, i.e. 63% of the annotated studies. For each of these
527 samples we calculated the fold-enrichment for each ChIP-seq sample compared to the inputs
528 or controls in the same cell type from within the same study. This data was then ranked from
529 most enriched protein to least enriched protein.

530 We first looked at the most enriched proteins for each locus and performed a number of quality
531 control checks based on technical and biological expectations. We looked at all of the samples
532 within a study containing an enriched protein, as we observed that problematic samples were
533 often contained within problematic studies. In most cases there was no reason for concern, but
534 examples where enriched-proteins would be excluded include studies with unusually low
535 input/control samples which gave spurious enrichment to all samples in the study, including
536 for proteins which are consistently not enriched in other studies. We also looked at instances
537 of a 'top hit protein' in other studies, and noted whether the protein had previously been
538 observed at centromeres in published manuscripts or whether the protein was a new candidate
539 locus-specific protein. We identified the most robust top-hit proteins by focussing on examples
540 that were strongly supported within single studies (i.e. enriched compared to other proteins
541 assayed) and/or across multiple studies.

542

543 ***REDPOINT validation using published datasets***

544 The BioProject accession number (PRJNA######) for each relevant study is included in the
545 figure legend or supplementary tables associated with each observation.

546

547 *Confirming the centromere localisation of top-hit proteins identified by REDPOINT*

548 To confirm the localisation of the top-hit centromere proteins we repeated the analysis using
549 the complete sequencing run. Each ChIP-seq sample was downloaded using 'fastq-dump' from
550 NCBI SRA Tools or directly from the SRA Explorer website (https://sra-explorer.info/). The
551 technical quality of each sample was assessed using FastQC. Each sample was then aligned to
552 the hg38 version of the human genome using Bowtie2 (ver.2.3.0), converted to .bam file using
553 samtools (ver.1.3.1) and to .bed file using BEDTools (ver.2.26). Aligned files were intersected
554 with a table of centromeric regions extracted from the hg38 genome build using the 'intersect'

555 function in BEDTools. The total number of aligned reads and the proportion aligned to different
556 repetitive regions, including centromeres, was calculated using custom bash scripts and
557 processed for visualisation in R using ggplot2.

558

559 *Visualising BRD4 as a centromere protein on a T2T genome*

560 To plot BRD4 and other centromere proteins across a complete chromosome we utilised the
561 recently published T2T genome build of human chromosome 8[4]. We followed the same
562 mapping strategy as outlined in the T2T publication[4], which utilises samtools (ver.1.3.1) and
563 the alignment package bwa (ver.0.7.17)[8] with the following parameters (bwa mem -k 50 -c
564 100000 PATH/CHM13.chr8.fasta FILE.fastq > FILE.sam). To convert .sam files to .bam we
565 used samtools sort with the following parameters (samtools sort FILE.sam -o FILE.bam) and
566 samtools index (samtools index FILE.bam). To plot the genomic distribution of BRD4 or other
567 centromeric proteins compared to corresponding input we utilised the bamCompare function
568 in BEDTools (ver.2.30.0) with the following parameters (bamCompare -b1 SAMPLE.bam -b2
569 INPUT.bam --scaleFactorsMethod SES --operation ratio --binSize 1000 --samFlagExclude
570 2308 --outFileFormat bedgraph -o NAME.bedGraph). The bedGraph files were uploaded to
571 the UCSC genome browser (https://genome.ucsc.edu/) and the 'mean' signal visualised with
572 smoothing set to 10.

573

574 *Identification and validation of JQ1-dependent increase in centromeric BRD4*

575 To validate BRD4-JQ1 as the most prominent hit we included additional ChIP-seq datasets
576 investigating BRD4 following JQ1 treatment which were missed in our annotated REDPOINT
577 data, giving a total of 15 analysed datasets. We followed the same approach outlined above to
578 confirm the centromere localisation using the hg38 and T2T genome. To visualise the fold
579 change in BRD4 localisation following JQ1 treatment on the T2T genome we utilised the
580 bamCompare function in BEDTools (ver.2.30.0) with the following parameters (bamCompare
581 -b1 JQ1_sample.bam -b2 DMSO_sample.bam --scaleFactorsMethod SES --operation log2 --
582 binSize 1000 --samFlagExclude 2308 --outFileFormat bedgraph -o NAME.bedGraph). The
583 bedGraph files were uploaded to the UCSC genome browser (https://genome.ucsc.edu/) and
584 the 'mean' signal visualised with smoothing set to 5. To further characterise the effect of JQ1

585 treatment on centromeric H3K27ac, RNA polymerase II and transcription we analysed ChIP-
586 seq and RNA-seq datasets using the same approaches.

587

588 *Chromosome specificity of BRD4 centromere recruitment by JQ1*

589 We analysed the enrichment of BRD4 following JQ1 at different annotated repeats within the
590 centromere to identify evidence for a central role of CENP-B in recruiting BRD4. We first set
591 out to determine if α-satellite DNA, which is the only centromeric satellite that contains the
592 CENP-B box DNA sequence, is the most enriched repeat class. To do this we aligned matched
593 BRD4-JQ1 and BRD4-DMSO samples to the hg38 genome build, intersected with the table of
594 repetitive regions extracted from hg38, and quantified the percentage of reads aligned to each
595 class of centromeric repeat. Next, we used the same data to focus on the chromosome-specific
596 breakdown of centromeric repeats that recruit BRD4 following JQ1 treatment. We calculated
597 the percentage of centromeric reads aligned to the centromere of each chromosome in each
598 sample. We then determined the ratio of JQ1 compared to DMSO for each centromere in
599 matched JQ1/DMSO pairs to focus on the relative change in BRD4-association across
600 centromeres, independent of centromere length or changes in the total level of BRD4 across all
601 centromeres. Finally, we compared the relative abundance of CENP-B on each centromere to
602 the enrichment of BRD4 following JQ1, using published CENP-B CUT&RUN and BRD4
603 ChIP-seq data. Enriched chromosomes contain more BRD4 and/or CENP-B than would be
604 expected based on the size of the centromere. The CENP-B data was generated in HeLa, a
605 female cell-line, therefore we cannot assay the Y-chromosome. As negative controls, we
606 compared centromeric CENP-B enrichment to RNA polymerase II JQ1/DMSO treatment and
607 BRD4 following degradation of BRD4 with a PROTAC inhibitor (dBET6/DMSO).

608

609 *Immunoprecipitation mass spectrometry analysis*

610 Processed BRD4 co-immunoprecipitation mass spectrometry (coIP-MS) data was obtained
611 from the supplementary information of two articles[9,10]. For SUM149/R cells the ratio of JQ1
612 to DMSO was calculated from the peptide level in the 'RIME filtered list' in Supplementary
613 Table S3, and our observations are consistent with data presented in Figure 1E of this study[10].
614 Data from HEK293T and K562 cells were calculated from Supplementary Table S2G and S2H
615 based on the fold-enrichment of each protein in the pull-down vs control[9]. The ratio of the JQ1

616 enrichment over the DMSO enrichment was used to identify the proteins most enriched upon
617 JQ1 treatment. Co-IP MS data from this study was also analysed for BRD2 and BRD3 to
618 determine the specificity of the identified drug-dependent protein complexes.

619

620 *Analysis of published CRISPR KO screen in SUM149/R cells*

621 Processed CRISPR KO screen data for SUM149 and JQ1-resistant SUM149R cells in the
622 presence DMSO or JQ1 were obtained from the Supplementary Information of a recent
623 resource article[10]. This data contained the p-values for the enrichment of cells containing each
624 protein-targeting sgRNA compared to control sgRNAs. Enriched sgRNAs have a positive
625 value and highlight proteins whose knock-out promotes cell proliferation, depleted sgRNAs
626 have a negative value and highlight proteins whose knock-out decreases cell proliferation. Our
627 analysis is broadly similar to Figure 1a in the source publication[10], and uses the same cut-off
628 of $p>0.001$ for candidate hits but focused on pathways which were not considered or
629 highlighted in the original publication, including proteins involved in centromere function, the
630 spindle assembly checkpoint and sister chromatid cohesion

631

632 *Producing Figures*

633 All data processing and presentation in boxplots, bar charts, line graphs and other forms of
634 graphical analysis was performed in R using standard tools and ggplot2. All
635 immunofluorescence, metaphase spread and western blot images were processed in ImageJ by
636 changing the brightness/contrast only. All figures were assembled in Affinity Designer.

637

638 *Statistical analyses*

639 All statistical analysis was performed in R or Excel and each test and p-value is outlined in the
640 associated legend for each figure.

641

642

643 ***Experimental procedures used in validation of REDPOINT results***

644 *Cell Culture*

645 Human cell lines HEK293T originally obtained from the American Type Culture Collection
646 (ATCC) and HeLa SNAP CENPA (referred to as HeLa cells) were obtained from the Fachinetti
647 lab (Institut Curie). Cells were cultured in DMEM (Gibco #61965-026) supplemented with
648 10% Foetal Bovine Serum (Capricorn scientific FBS-12A), 1% penicillin/streptomycin
649 (Capricorn scientific PS-B) and sodium pyruvate at a final concentration of 1mM.

650

651 *Bromodomain inhibitor treatment*

652 HEK293T and HeLa cells were treated with 0.25% DMSO (Sigma D8418) or bromodomain
653 inhibitors dissolved in DMSO to give a final concentration of 0.25% DMSO plus inhibitor.
654 Cells were treated for 1 hour or 24 hours, stated in the figure legends, with 500nM JQ1 (Sigma
655 SML0974), 500nM JQ1 (+) or (-) enantiomers (Millipore 500586) or 5μM PFI1 (Torris 4445),
656 a bromodomain inhibitor with a distinct structure and mechanism of action to JQ1 that requires
657 10x higher concentration for the same reduction in cell growth[11]. In addition, BRD4
658 degradation was achieved by 24 hours incubation with the PROTAC Inhibitor 500nM MZ1
659 (provided by Boehringer Ingelheim opnMe portal).

660

661 *Immunofluorescence*

662 HEK293T or HeLa cells were seeded on coverslips in 6-well plates and incubated at least
663 overnight to enable cells to settle and grow on the surface. Cover slips were washed gently
664 once in PBS followed by 7 minutes fixation in 4% PFA, 3x 5-minutes wash in PBS,
665 permeabilization in 0.3% Triton X-100 for 7 minutes and 3x 5-minutes PBS wash. Fixed cells
666 were blocked in 1% BSA in PBS for 30 minutes at room temperature before overnight
667 incubation at 4°C in primary antibodies: α-mouse CENP-A (1:1000 Abcam ab13939
668 (discontinued) or 1:1500 Enzo ADI-KAM-CC006-E) and α-rabbit BRD4 (1:900 Abcam
669 ab128874). The following day fixed cells were washed 3x 10-minutes in PBS and then
670 incubated 1 hour in secondary antibodies (Alexa Fluor 488, 546 or 647) before 3x 10-minute
671 wash in PBS, 5 minutes incubation in DAPI solution to stain the DNA, 1x PBS wash and mount
672 slide/coverslip with Aqua Poly Mount (Polysciences Inc. 18606-20). Imaging was performed

673 on a Zeiss AiryScan2 LSM900 confocal microscope using the 'airyscan mode' and following
674 standard operating procedures[12].

675

676 *BRD4 co-IP*

677 HEK293T or HeLa cells were split into 1x 10cm dish per IP and allowed to grow overnight
678 before treatment with DMSO, 500nM JQ1 or 5μM PFI1 for 1 hour. We utilised the Active
679 Motif Nuclear Complex Co-IP kit (#54001) following the manufacturer's instructions with the
680 following variations: we incubated the 'enzyme shearing cocktail' for 2 minutes at 37°C, we
681 used the 'gentle IP buffer' to wash samples. The immunoprecipitation antibody was α-rabbit
682 BRD4 (Bethyl A301-985-A-M).

683

684 *Western blot analysis*

685 Standard western blot procedures were followed for the quantification of protein abundance in
686 a variety of samples including following BRD4 co-IP. Briefly protein samples were prepared
687 from experimental samples or cell pellets by resuspending in 1x final concentration Laemmli
688 solution, followed by water bath sonication (Diagenode Bioruptor Plus) to reduce sample
689 viscosity and a 5-minute incubation at 95°C to ensure complete protein denaturation. Samples
690 were loaded on a 4-15% gradient gel (Bio-Rad 4561083) and run at 150v for 1 hour (Bio-Rad
691 system). The protein was transferred to PVDF membrane (Amersham 10600022) using semi-
692 dry transfer apparatus using the 'mixed MW' setting (Bio-Rad trans blot turbo). Membranes
693 were blocked for 1 hour in 5% powdered milk in TBS-T, followed by overnight primary
694 antibody incubation at 4°C. Primary antibodies used: α-mouse CENP-A (1:1000 Abcam
695 ab13939 (discontinued) or 1:1500 Enzo ADI-KAM-CC006-E), α-rabbit CENP-B (1:500
696 Abcam ab25734), α-rabbit CENP-C (1:50 Abcam ab193661), β-actin (Sigma A3854) and α-
697 rabbit BRD4 (1:500 Bethyl A301-985-A-M). Following overnight incubation membranes were
698 washed 3x 10-minutes in TBS-T, then incubated in α-mouse-HRP (Sigma A9044) or α-rabbit-
699 HRP (Sigma A0545) in 5% milk for 1 hour at room temperature. Membranes were then washed
700 3x 10-minutes in TBS-T followed by a brief incubation in ECL reagent. Chemiluminescence
701 was detected using chemiluminescent substrate (Thermo 34095 or 34575).

702

703 *Generating CENP-B CRISPR KO cell lines*

704 CRISPR KO cell lines and matched 'safe guide' controls were generated in HEK293T and
705 HeLa cells using lentivirus-mediated gene KO. HEK293T cells were also used to produce the
706 lentivirus. The first step towards generating CENP-B KO cell lines was to establish CAS9
707 stable cell lines for HEK293T and HeLa cells. Cell lines were transduced with lentiCas9-
708 Blast[13] (Addgene, #52962) and selected with 20 µg/ml blasticidin to generate stable CAS9-
709 expressing cell lines. sgRNA for CRISPR KO were designed using the Sanjana lab tool
710 (http://guides.sanjanalab .org/) and cloned as previously described[5,16]. Briefly, sgRNAs were
711 cloned by annealing two DNA oligos and ligating into a BsmB1-digested pLKO1-puro-U6-
712 sgRNA-eGFP. This construct was transformed into Stbl3 bacteria. For virus production 1
713 million HEK293T cells were transfected with 3 µg of the pLKO1-puro-U6-sgRNA-eGFP
714 plasmid and two helper vectors (2.5 µg psPAX2 and 0.9 µg VSV-G). Packaging cells were
715 transfected using polyethyleneimine (Polysciences, 23966-2) by mixing with DNA in a 3:1
716 ratio. 48 hours post-transfection viral supernatants were collected, filtered through a 0.45 µm
717 filter and supplemented with 4 µg /ml of polybrene (Sigma) before adding to target cells.
718 Downstream experiments using sgRNA KO were performed on the pool after at least 10 days,
719 or on single-cell clones that were isolated from the pool.

720

721 *Quantifying centromere cohesion defects on metaphase spreads*

722 Metaphase spreads were prepared using a standard method for karyotype analysis using
723 Carnoy's fixative and dropping the sample onto a microscope slide[15]. This process produces
724 high resolution metaphase chromosome features, but under these fixation conditions
725 centromeric antibodies do not detect their epitope[16], which prevents fluorescence microscopy.
726 Briefly, 1 well of a 6-well plate per sample was seeded two days prior to metaphase
727 chromosome preparation. 24 hours prior to metaphase chromosome preparation cells were
728 treated with DMSO or BET bromodomain inhibitors (JQ1, MZ1). 2 hours prior to metaphase
729 chromosome preparation cells were treated with 1µg/ml colcemid. Cells were then harvested,
730 combining the media, wash and cells into a single 15ml Falcon tube. To swell cells were
731 resuspended in 5ml 75mM KCl for 10-minutes at room temperature. Cells were pelleted by
732 centrifugation and resuspended in 10ml Carnoy's fixative (3-parts methanol to 1-part acetic
733 acid) and incubated for 10 minutes at room temperature. This pelleting, resuspending and
734 incubation was repeated twice more and samples were then placed at -20°C at least over-night,

735 and maintained at -20°C for long term storage. To prepare slides of metaphase chromosomes,
736 samples were recovered from -20°C storage, cells pelleted by centrifugation, resuspended in
737 10ml room temperature Carnoy's fixative, incubated for 10 minutes at room temperature,
738 pelleted and resuspended in a small amount of Carnoy's fixative dependent on the pellet size.
739 To drop the slides we took 20 µL of the sample, hydrated the surface of a positively charged
740 microscope slide (Hecht 42409110) with a gentle open mouthed blow, and quickly dropped the
741 sample from a height of approximately 10 cm. Slides were allowed to dry overnight in a dark
742 drawer. The following day slides were rehydrated for 5 minutes in PBS, incubated in DAPI
743 and mounted using Aqua Poly Mount. Imaging was performed on an Zeiss AiryScan2 LSM900
744 confocal microscope using the 'airyscan mode' and following standard operating procedures.
745 Metaphase imaging and analysis was performed blind and the categorisation of centromere
746 defects was based on published observations[17]

747

748 *In vitro reconstitution of the BRD4-JQ1-CENP-B-DNA interaction*

749 To identify whether the BRD4-JQ1-CENP-B-DNA interaction can be reconstituted *in vitro* we
750 purchased or purified each component of the complex. We purchased custom pairs of oligos
751 (Sigma) that can be annealed to form double stranded DNA, and with a 5' biotin on the forward
752 oligo, for a sequence that has been previously characterised to bind CENP-B *in vitro*[18] (F primer
753 – GGCCTTCGTTGGAAACGGGATTT) and a shuffled version of the same sequence as a
754 negative control for CENP-B binding (F primer – GTTAGCGATTTGAATTCCGGGGC).
755 Full-length purified CENP-B was purchased from Active Motif (No. 81201) and JQ1 (+) or (-
756) enantiomers were purchased from Sigma (SML1524 & SML1525).

757 Sumo tagged BRD4^{bromo} (44-460 aa) was expressed in BL21 *E. coli* after induction with IPTG
758 overnight at 15°C and purified using an ÄKTA pure first with a nickel column (Cytivia HisTrap
759 HP 17524701), followed by a buffer exchange (Cytivia HiTrap Desalting 17140801), Ulp1
760 cleavage [19] and a second round of nickel chromatography to remove the SUMO tag. Protein
761 purity was determined by Coomassie stained SDS PAGE and aliquots flash frozen in liquid
762 nitrogen.

763 To prepare the magnetic beads, 15µl Dynabeads MyOne Streptavidin T1 beads (Invitrogen
764 65601) were resuspended in 100µl Binding and Wash (BW) Buffer (5mM Tris-HCl pH7.5,
765 0.5mM EDTA, 1M NaCl). A magnetic rack was used to separate the beads and the supernatant

766 was discarded. Beads were washed 3x in BW buffer, using the rack to separate the beads and
767 discarding the supernatant each time.

768 Double stranded DNA was prepared by resuspending complementary oligonucleotides in
769 annealing buffer (5mM Tris-HCl pH6.8, 1mM EDTA, 50mM KCl, 0.01% triton X-100),
770 heating to 95°C for 5 minutes followed by cooling the samples at 1°C per minute until 4°C.
771 30pmol of dsDNA was resuspended in Binding and Wash (BW) Buffer (5mM Tris-HCl pH7.5,
772 0.5mM EDTA, 1M NaCl) to a total volume of 100µl. This DNA was added to the pre-washed
773 streptavidin beads and incubated for 30 minutes at 24°C with gentle shaking to immobilise the
774 biotinylated dsDNA on the beads. The beads were then washed one time in BW Buffer and
775 twice in Binding Buffer (20mM HEPES pH7.6, 10% glycerol, 1mM EDTA, 3mM DTT, 0.05%
776 NP40, 150mM NaCl). Following the final wash beads were resuspended in 30µl Binding
777 Buffer containing 2.5 pmol CENP-B, 25 pmol $BRD4^{bromo}$ and 50 pmol (+)-JQ1 or (-)-JQ1. An
778 Input sample 3µl (10%) aliquot was taken and frozen, the remainder of the sample was
779 incubated overnight at 4°C rotating at 20rpm. The following day Binding Buffer was added to
780 a final volume of 300µl, the tube incubated on a magnetic rack, as a Flow Through sample a
781 30µl (10%) aliquot was taken and frozen, and the remaining supernatant was discarded. The
782 beads were then washed three more times in 300µl Binding Buffer, with a 30µl (10%) aliquot
783 of the Final Wash taken and frozen. After the final wash 30µl 1x Laemmli buffer was added to
784 the beads to give the Complex sample. Each of the Input samples was made up to 30µl in
785 Binding Buffer and 10µl of 4x Laemmli buffer was added to the Input, Flow Through and Final
786 Wash samples. All of the samples were boiled at 95°C for 5 minutes, centrifuged and loaded
787 on 10% SDS PAGE gels for Western Blot. Western blot was performed as outlined previously
788 with primary antibodies to BRD4 (Abcam ab128874) and CENP-B (Abcam ab25734).

789

790 **Data and code availability:** All data are available in the main text or the supplementary
791 materials. REDPOINT approach utilizes standard analysis tools as described in methods, code
792 available on request.

793

794

795

796 **Methods references**

797 1. Katz, K. *et al.* The Sequence Read Archive: a decade more of explosive growth. *Nucleic*
798 *Acids Res* **50**, D387–D390 (2022).

799 2. Miga, K. H. The Promises and Challenges of Genomic Studies of Human Centromeres.
800 *Prog. Mol. Subcell. Biol.* **56**, 285–304 (2017).

801 3. Altemose, N. *et al.* Complete genomic and epigenetic maps of human centromeres.
802 *Science* **376**, eabl4178 (2022).

803 4. Logsdon, G. A. *et al.* The structure, function and evolution of a complete human
804 chromosome 8. *Nature* **593**, 101–107 (2021).

805 5. Langmead, B. & Salzberg, S. L. Fast gapped-read alignment with Bowtie 2. *Nat*
806 *Methods* **9**, 357–359 (2012).

807 6. Anders, S., Pyl, P. T. & Huber, W. HTSeq--a Python framework to work with high-
808 throughput sequencing data. *Bioinformatics* **31**, 166–169 (2015).

809 7. Henikoff, S., Henikoff, J. G., Sakai, A., Loeb, G. B. & Ahmad, K. Genome-wide
810 profiling of salt fractions maps physical properties of chromatin. *Genome Res.* **19**, 460–469
811 (2009).

812 8. Li, H. & Durbin, R. Fast and accurate long-read alignment with Burrows-Wheeler
813 transform. *Bioinformatics* **26**, 589–595 (2010).

814 9. Lambert, J.-P. *et al.* Interactome Rewiring Following Pharmacological Targeting of
815 BET Bromodomains. *Mol Cell* **73**, 621-638.e17 (2019).

816 10. Shu, S. *et al.* Synthetic Lethal and Resistance Interactions with BET Bromodomain
817 Inhibitors in Triple-Negative Breast Cancer. *Mol Cell* **78**, 1096-1113.e8 (2020).

818 11. Picaud, S. *et al.* PFI-1, a highly selective protein interaction inhibitor, targeting BET
819 Bromodomains. *Cancer Res* **73**, 3336–3346 (2013).

820 12. Wu, X. & Hammer, J. A. ZEISS Airyscan: Optimizing Usage for Fast, Gentle, Super-
821 Resolution Imaging. *Methods Mol Biol* **2304**, 111–130 (2021).

822 13. Sanjana, N. E., Shalem, O. & Zhang, F. Improved vectors and genome-wide libraries
823 for CRISPR screening. *Nat Methods* **11**, 783–784 (2014).

14. Shalem, O. *et al.* Genome-scale CRISPR-Cas9 knockout screening in human cells. *Science* **343**, 84–87 (2014).

15. Hliscs, R., Mühlig, P. & Claussen, U. The spreading of metaphases is a slow process which leads to a stretching of chromosomes. *Cytogenet Cell Genet* **76**, 167–171 (1997).

16. Beh, T. T., MacKinnon, R. N. & Kalitsis, P. Active centromere and chromosome identification in fixed cell lines. *Mol Cytogenet* **9**, 28 (2016).

17. Nagasaka, K. *et al.* Cohesin mediates DNA loop extrusion and sister chromatid cohesion by distinct mechanisms. *bioRxiv* 2022.09.23.509019 (2022) doi:10.1101/2022.09.23.509019.

18. Muro, Y. *et al.* Centromere protein B assembles human centromeric alpha-satellite DNA at the 17-bp sequence, CENP-B box. *J Cell Biol* **116**, 585–596 (1992).

19. Kuo, D., Nie, M. & Courey, A. J. SUMO as a solubility tag and in vivo cleavage of SUMO fusion proteins with Ulp1. *Methods Mol Biol* **1177**, 71–80 (2014).

Acknowledgements

We would like to acknowledge the bwForCluster Helix and MLS&WISO for computational infrastructure and support. We would like to thank Iain Cheeseman, Andrea Mussachio and Christopher Playfoot for critical feedback on the manuscript and Daniele Fachinetti, Aubry Miller and the Erhardt lab for valuable comments and discussion.

Funding:

Deutsche Forschungsgemeinschaft (DFG) grant EXC81 (CellNetworks) (SE)

Deutsche Forschungsgemeinschaft (DFG) grant GRK2039 (SE)

European Research Council grant ERC-CoG-682496 (cenRNA) (SE)

European Research Council grant grant nº805338 (AB, NSB)

DKFZ Postdoctoral Fellowship (NSB)

Deutsche Forschungsgemeinschaft (DFG) grant INST 35/1597-1 FUGG

Deutsche Forschungsgemeinschaft (DFG) grant INST 35/1134-1FUGG

Author contribution:

Conceptualization: SC, SE

Data curation: SC, NPS

Methodology: SC, NPS, NSB, JB, AMS, VD, SA

Investigation: SC, NSB, JB, AMS, VD

Visualization: SC, NSB, SE

Funding acquisition: SE, AB, NSB

Project administration: SC, SE

Supervision: SC, SE, SA

Writing – original draft: SC, SE

Writing – review & editing: SC, SE, NSB, AB, SA, JB, AMS, VD

Competing Interests: Authors declare that they have no competing interests.

Corresponding Author: Sylvia.Erhardt@KIT.edu

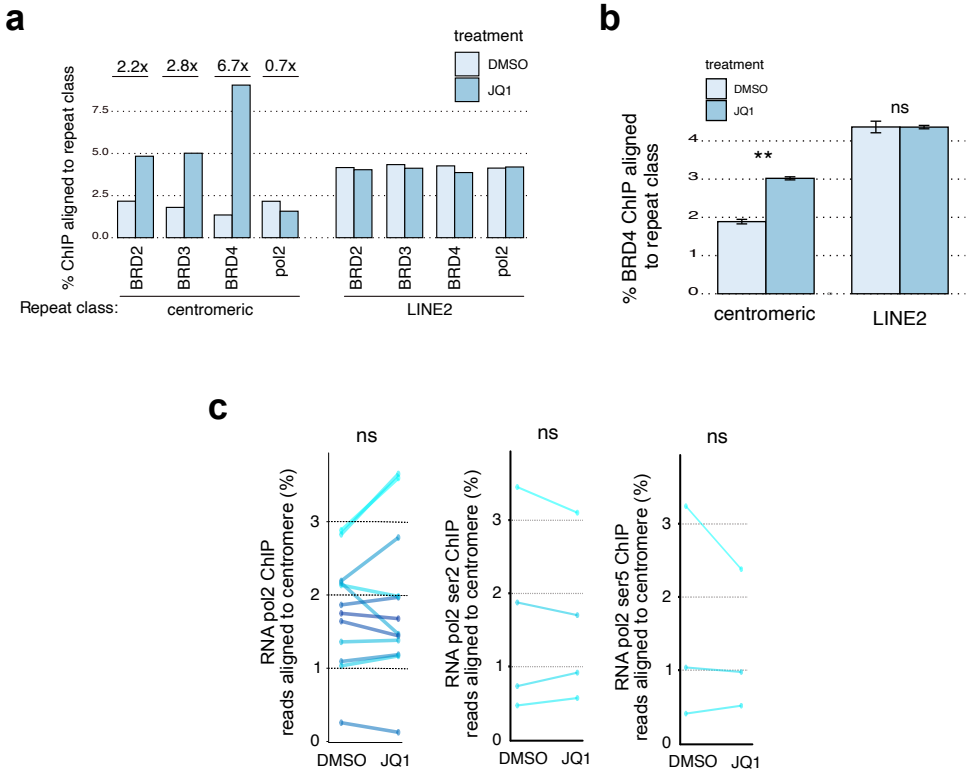

Extended Data Fig. 1 | BRD4 is specifically enriched at centromeres following JQ1 treatment, but does not recruit RNA polymerase II. a, Centromeric alignment level of BRD2, BRD3, BRD4 and POL2 at centromeres and LINE2 elements following DMSO or JQ1 treatment. Data from: PRJNA253142. **b**, Centromeric alignment level of BRD4 at centromeres and LINE2 elements in a dataset with quadruplicate samples following DMSO or JQ1 treatment. Error bars = standard error of the mean. Statistical analysis t-test (ns 'not significant', ** $p<0.01$). Data from PRJNA482365. **c**, Centromeric alignment of RNA polymerase II following DMSO or JQ1 treatment from multiple studies. Total pol2 – 12 studies, pol2 ser2 – 4 studies, pol2 ser5 – 3 studies. For full data see Supplementary Table 13.

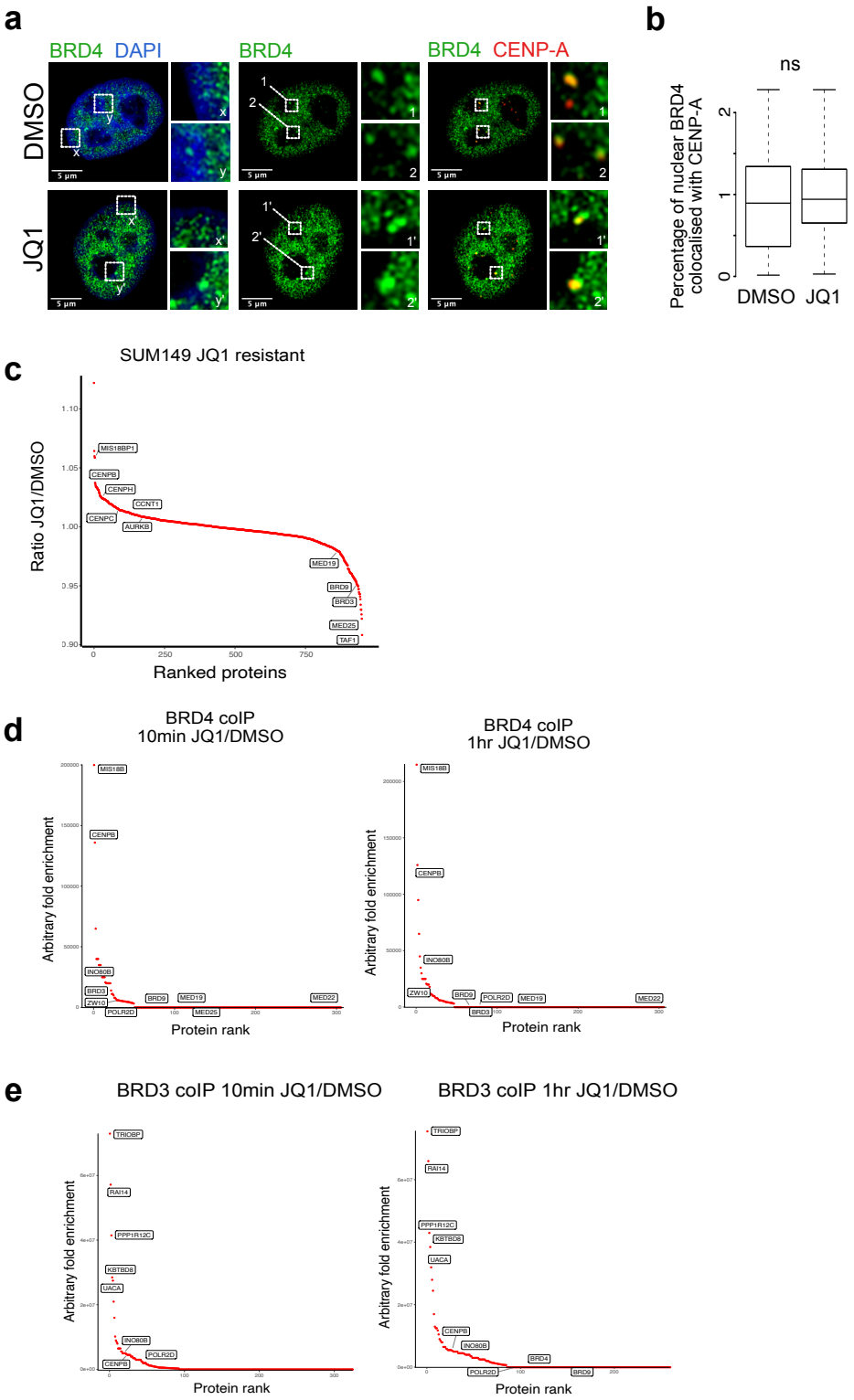
a
BRD4 DAPI
BRD4
BRD4 CENP-A
DMSO
JQ1
b
ns
Percentage of nuclear BRD4 colocalised with CENP-A
DMSO JQ1
c
SUM149 JQ1 resistant
Ratio JQ1/DMSO
Ranked proteins
MIS18BP1
CENPB
CENPH
CCNT1
CENPC
AURKB
MED19
BRD9
BRD3
MED25
TAF1
d
BRD4 coIP
10min JQ1/DMSO
BRD4 coIP
1hr JQ1/DMSO
Arbitrary fold enrichment
Protein rank
MIS18B
CENPB
INO80B
BRD3
ZW10
POLR2D
BRD9
MED19
MED25
MED22
e
BRD3 coIP 10min JQ1/DMSO
BRD3 coIP 1hr JQ1/DMSO
Arbitrary fold enrichment
Protein rank
TRIOBP
RAI14
PPP1R12C
KBTBD8
UACA
INO80B
POLR2D
CENPB
BRD4
BRD9

882

883

884

885

886

887

888

889

890

891

892

893

894

895

896

897

898

899 **Extended Data Fig. 2 | JQ1 stabilises a complex containing BRD4 and centromeric**
900 **proteins. a**, Immunofluorescence imaging of BRD4 (green) and CENP-A (red) in HeLa cells
901 following 24 hours DMSO or (±)-JQ1 treatment. BRD4/DAPI inset images highlight the
902 nuclear periphery (x and x') and the nucleolar periphery (y and y'). BRD4 and BRD4/CENP-
903 A inset images (1, 1', 2 and 2') highlight core-centromere locations (CENP-A enriched). **b**,
904 Quantification of the percentage of total nuclear BRD4 signal which co-localises with CENP-
905 A in DMSO or (±)-JQ1 treated HeLa cells. Statistical test is a t-test (n=90 cells for DMSO and
906 90 cells for JQ1). **c**, BRD4 co-IP MS in SUM149R cells comparing proteins enriched in JQ1
907 compared to DMSO, with key proteins for centromere identity and BRD4-mediated
908 transcription regulation highlighted. Data from Shu et al. (2020)[28]. **d**, BRD4 co-IP MS in
909 HEK293T cells comparing proteins enriched in JQ1 compared to DMSO after 10 minutes or
910 one-hour inhibitor treatment. Data from Lambert *et al*. 2019. **e**, BRD3 co-IP MS in HEK293T
911 cells comparing proteins enriched in JQ1 compared to DMSO after 10 minutes or one-hour
912 treatment. Data from Lambert *et al*. 2019[29].

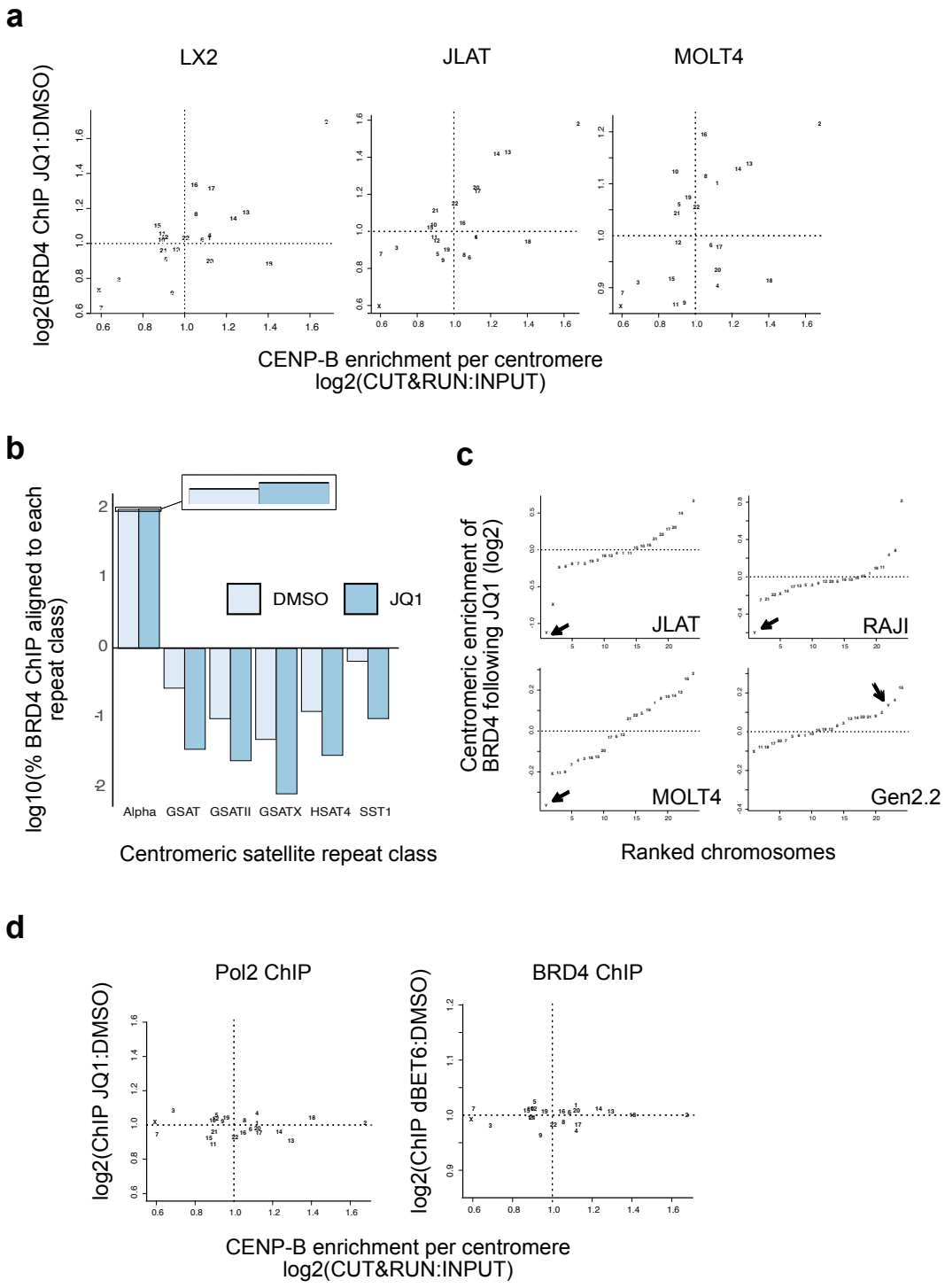
a
LX2
JLAT
MOLT4
log2(BRD4 ChIP JQ1:DMSO)
CENP-B enrichment per centromere
log2(CUT&RUN:INPUT)
b
log10(% BRD4 ChIP aligned to each repeat class)
DMSO
JQ1
Alpha
GSAT
GSATII
GSATX
HSAT4
SST1
Centromeric satellite repeat class
c
Centromeric enrichment of BRD4 following JQ1 (log2)
JLAT
RAJI
MOLT4
Gen2.2
Ranked chromosomes
d
Pol2 ChIP
BRD4 ChIP
log2(ChIP JQ1:DMSO)
log2(ChIP dBET6:DMSO)
CENP-B enrichment per centromere
log2(CUT&RUN:INPUT)

913

914

915

Extended Data Fig. 3 | BRD4 is specifically enriched at CENP-B binding sites following JQ1 treatment. a, Relationship between CENP-B enrichment at each centromere and BRD4 recruitment following JQ1. CENP-B CUT&RUN data from PRJNA546288. BRD4 data: LX2 PRJNA253142, JLAT PRJNA391180, MOLT4 PRJNA315416. **b**, Quantifying the percentage of reads aligning to each class of centromeric DNA repeat. Whiskers = boxplot standard in R (1.5x IQR). Data in LX2 cells from data from PRJNA253142. **c**, ChIP-seq analysis of centromeres ranked by BRD4 enrichment following JQ1 treatment in male cell lines. Enrichment was calculated by identifying the percentage of centromeric BRD4 at each chromosome in a sample, and then calculating the ratio of JQ1 treated sample compared to DMSO treated sample. The arrow indicates the Y chromosome. Data: JLAT PRJNA391180, RAJI PRJNA306758, MOLT4 PRJNA315416, Gen2.2 PRJNA306431. **d**, Correlation between CENP-B enrichment at each centromere and RNA polymerase II following JQ1 or BRD4 following BRD4 degradation with dBET6. Data: pol2 PRJNA253142, dBET6 PRJNA315416.

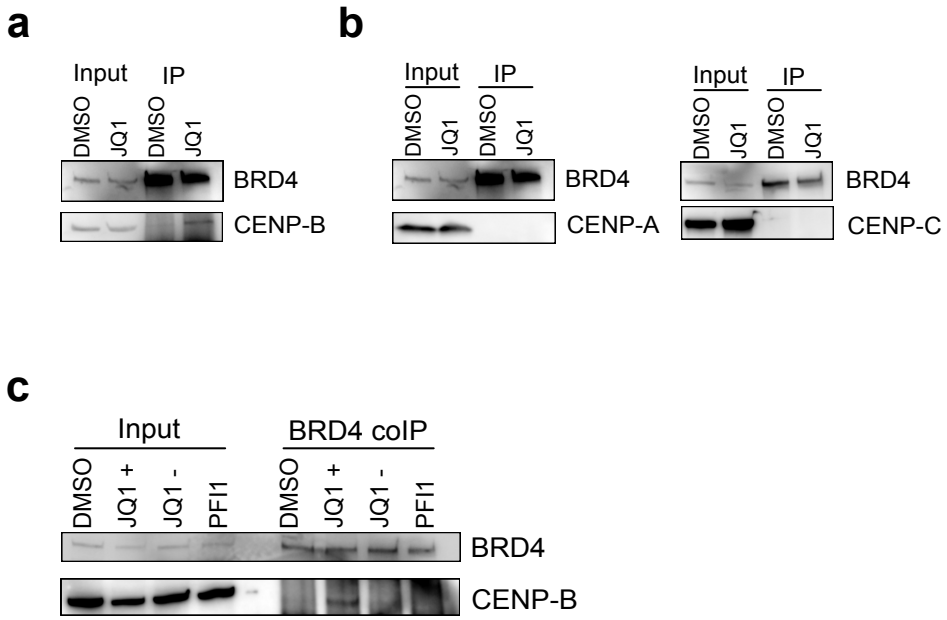

Extended Data Fig. 4 | A specific interaction occurs between BRD4 and CENP-B. a, Co-IP for BRD4 following DMSO or (±)-JQ1 treatment for 1 hour in HEK293T cells, followed by western blot for BRD4 and CENP-B. **b**, Co-IP for BRD4 following DMSO or (±)-JQ1 treatment for 1 hour in HeLa cells, followed by western blot for BRD4 and CENP-A or CENP-C. **c**, Co-IP for BRD4 following DMSO, (+)-JQ1, (–)-JQ1 or PFI1 treatment for 1 hour in HeLa cells, followed by western blot for BRD4 and CENP-B.

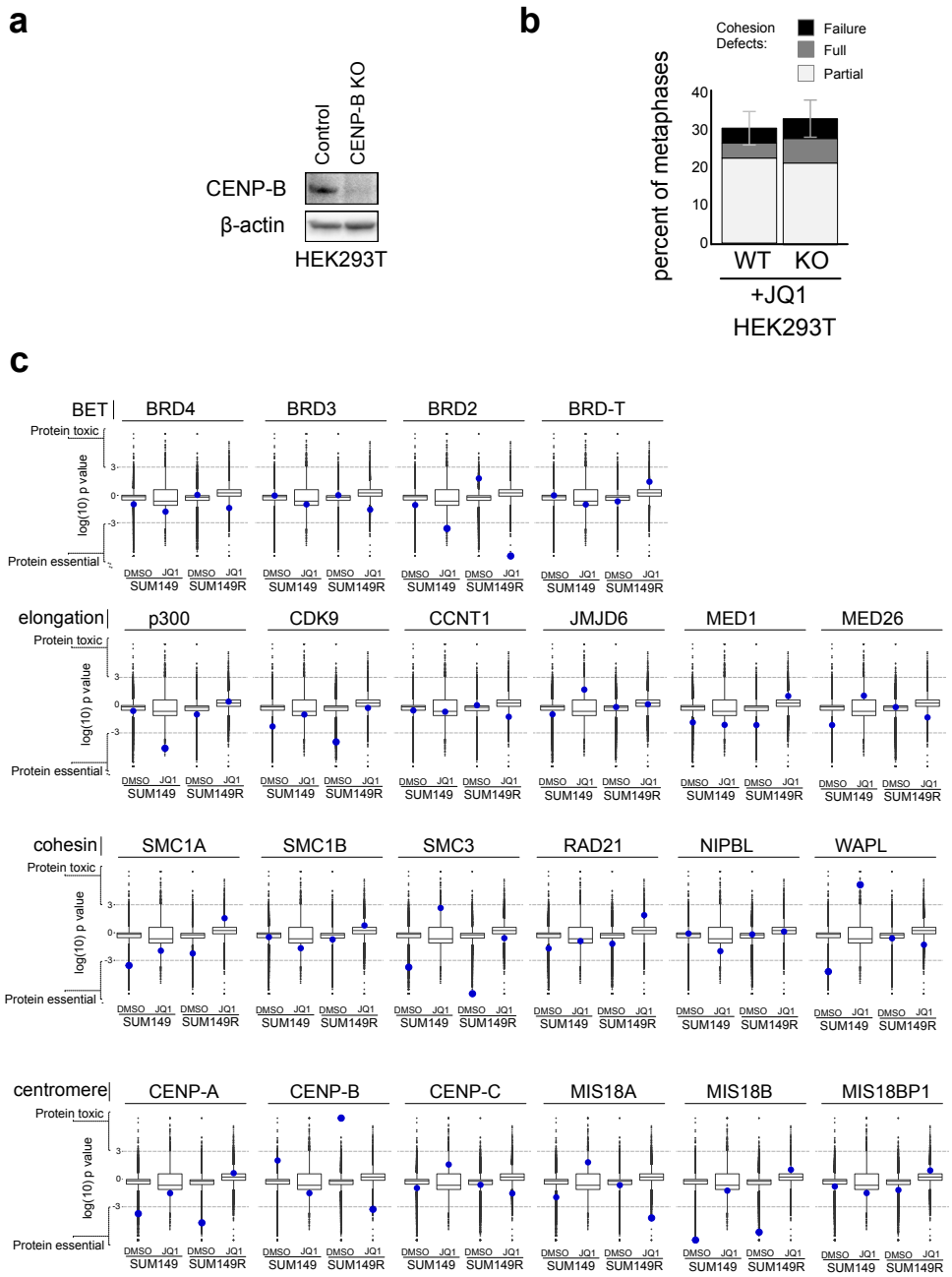
a
Control
CENP-B KO
CENP-B
β-actin
HEK293T
b
Cohesion Defects:
Failure
Full
Partial
percent of metaphases
40
30
20
10
0
WT
KO
+JQ1
HEK293T
c
BET
BRD4
BRD3
BRD2
BRD-T
elongation
p300
CDK9
CCNT1
JMJD6
MED1
MED26
cohesin
SMC1A
SMC1B
SMC3
RAD21
NIPBL
WAPL
centromere
CENP-A
CENP-B
CENP-C
MIS18A
MIS18B
MIS18BP1
Protein toxic
Protein essential
log(10) p value
3
0
-3
DMSO
JQ1
SUM149
SUM149R

959

960

961

962
963
964
965
966
967
968
969
970
971
972
973
974
975
976
977
978
979 **Extended Data Fig. 5 | CENP-B has a key role in JQ1-resistance. a**, Western blot confirming
980 CENP-B depletion in CENP-B KO in HEK293T cells. **b**, Quantification of cohesion defects
981 following 24 hours (±)-JQ1 treatment in HEK293T control (WT) and CENP-B KO cells. Error
982 bars = standard error of the mean. Statistical analysis based on triplicate experiments t-test (ns
983 'not significant'). **c**, CRISPR KO screen comparing the effect of different BET bromodomain
984 proteins, transcription elongation proteins, cohesin proteins and centromeric proteins relative
985 to 18,460 other proteins on cellular proliferation in JQ1-sensitive and -resistance SUM149
986 breast cancer cells. Data from Shu et al. (2020)[28]. Toxic proteins are those in which KO
987 promotes growth, essential proteins are those where KO reduces growth.